Theoretical and Experimental Comparison of Three Pumping Methods for Thulium Fiber Lasers for Low-Output Power (<10 W)

photonics

MDPI

Article

Theoretical and Experimental Comparison of Three Pumping Methods for Thulium Fiber Lasers for Low-Output Power (<10 W)

Anna Mauro [1], Valentina Serafini [1], Chiara Bellezza Prinsi [1], Matteo Cavagnetto [1], Luca Maggio Tanasi [2], Sabina Zaimovic [2], José Maria Blanco Triana [2], Gabriella Motta [2] and Guido Perrone [1,*]

[1] Dipartimento di Elettronica e Telecomunicazione, Politecnico di Torino, Corso Duca degli Abruzzi 24, 10129 Torino, Italy; anna.mauro@polito.it (A.M.); valentina.serafini@polito.it (V.S.); chiara.bellezza@polito.it (C.B.P.); matteo.cavagnetto@polito.it (M.C.)

[2] Alite s.r.l., Via Conte Rosso 3, 10121 Torino, Italy; luca.maggio@alitegroup.eu (L.M.T.); sabina.zaimovic@alitegroup.eu (S.Z.); jose.blanco@alitegroup.eu (J.M.B.T.); gabriella.motta@alitegroup.eu (G.M.)

* Correspondence: guido.perrone@polito.it

Abstract: Over the last decade, the number of demonstrations of Tm-doped fiber lasers has increased rapidly thanks to the applications of 2 µm fiber laser in sensing, surgery, and polymer processing. In the literature, there is plenty of evidence that increasing the output power and the efficiency of this class of fiber lasers is of interest to the scientific and industrial communities. This article presents a theoretical and experimental study on three possible pumping methods for a Tm-doped fiber laser: out-of-band pumping, using a semiconductor-based module emitting at 793 nm; in-band pumping, using an ad hoc homemade fiber laser emitting at 1600 nm; an intracavity configuration, in which in the pump light is generated within the laser cavity itself. This work demonstrates how applying alternative pumping methods does not lead to significant improvements in laser performance without first taking into account the losses introduced in the system when switching from a cladding-pumped to a core-pumped configuration.

Keywords: thulium fiber laser; in-band pumping; core pumping

Received: 28 February 2025
Revised: 26 March 2025
Accepted: 27 March 2025
Published: 1 April 2025

Citation: Mauro, A.; Serafini, V.; Bellezza Prinsi, C.; Cavagnetto, M.; Maggio Tanasi, L.; Zaimovic, S.; Blanco Triana, J.M.; Motta, G.; Perrone, G. Theoretical and Experimental Comparison of Three Pumping Methods for Thulium Fiber Lasers for Low-Output Power (<10 W). *Photonics* **2025**, *12*, 328. https://doi.org/10.3390/photonics12040328

1. Introduction

Fiber lasers (FLs) have revolutionized numerous fields of application, offering significant advantages, such as higher reliability, enhanced mechanical robustness, superior thermal management, simplified cavity alignment, and the ability to achieve nearly ideal beam quality [1–3]. Additionally, their intrinsic fiber-based design enables simplified and flexible beam delivery. Owing to these benefits, FLs—particularly ytterbium-doped fiber lasers—have become the dominant choice for industrial applications, being capable of delivering multi-kilowatt-output power in continuous-wave (CW) operation while maintaining a single-mode output beam, thus with the highest possible beam quality [4–6].

Recently, thulium fiber lasers (TFLs) have gained significant interest within the scientific community due to their efficient emission in the 1.8-to-2.1 µm wavelength range, which is particularly important for applications in environmental sensing [7,8], surgical procedures, and industrial processes. For instance, TFLs have been clinically studied for kidney stone treatment via lithotripsy [9–11], demonstrating superior reliability and efficiency compared with traditional Ho:YAG laser-based procedures [12,13]. Additionally, their emission around 2 µm enables the additive-free laser welding of polymers, a crucial

advantage for biomedical applications where toxic additives would otherwise prohibit laser welding [14,15]. Beyond the medical field, TFLs are widely used in wind shear detection radars, remote sensing, atmospheric pollution monitoring, and range-finding technologies [16,17].

TFLs are typically pumped near the 793 nm absorption peak, thanks to the availability of reliable high-power semiconductor lasers emitting at this wavelength and despite the large energy gap between the pump and emission wavelengths and therefore large quantum defect $q = 1 - \lambda_s/\lambda_p$. Energy transfer processes such as cross-relaxation can significantly enhance the overall efficiency of this system up to 82% by exciting two Tm^{3+} ions with a single pump photon at 793 nm [18]. However, since high-power laser diodes are inherently multi-mode, a double-clad fiber geometry is necessary to efficiently couple the multi-mode pump while obtaining an output with high beam quality typical of a single-mode laser [19]. The use of this fiber geometry implies quite long active fiber lengths due to the weak overlap between the pump and dopant distributions. Consequently, this not only affects the compactness of the system but also imposes significant limitations in pulsed operation regimes, such as Q-switching, because longer fiber lengths increase cavity round-trip time, which can negatively impact pulse shaping and energy efficiency [20]. Beyond these structural constraints, pumping at 793 nm introduces more critical drawbacks. The high inversion levels generated at this wavelength can lead to parasitic up-conversion via Excited-State Absorption (ESA), which competes with the lasing process and reduces output efficiency [21]. Additionally, quenching effects contribute to excessive heat generation in the fiber core, further degrading performance. Finally, while cross-relaxation is beneficial for long-wavelength emission around 2 µm, it negatively impacts shorter-wavelength lasing in the 1.8-to-1.9 µm range, limiting the laser's efficiency in this spectral region.

An alternative approach that further enhances the efficiency of Tm-doped fiber lasers (TFLs) is pumping closer to the 1600 nm absorption peak of Tm^{3+}, also described in the literature as in-band pumping [22,23]. A smaller difference between the pump and signal wavelengths significantly reduces heat generation, leading to improved thermal management and higher overall laser efficiency. While pumping at 793 nm relies on cross-relaxation for increasing efficiency, a 1600 nm pump directly excites the upper laser energy level $^3H_4$, eliminating lossy conversions and achieving a quantum efficiency of almost 90%. The main limitation of 1600 nm pumping is the lack of commercially available high-power semiconductor laser diodes emitting at this wavelength. We address this issue by generating the 1600 nm pump directly from an erbium–ytterbium (Er/Yb) co-doped fiber laser, with the additional advantage of using single-mode (or near-single-mode) emission, which is also guided by the core of the Tm^{3+}-doped fiber, enabling a core-pumped configuration. The combination of in-band and core pumping allows for a substantial reduction in the length of Tm^{3+} active fiber necessary, improving compactness and efficiency. These novelties address the main issues that are currently limiting pulsed operation regimes such as Q-switching, which is ultimately the main motivation and future application of this work.

This pumping scheme can be implemented in two ways, namely, tandem pumping and intracavity pumping [24]. The former uses an Er/Yb fiber laser as the pump source, while the latter involves designing a laser cavity with two different fibers, an Er/Yb-doped fiber of length L_{ErYb} and a Tm-doped fiber of length L_{Tm}. Although some examples of these configurations can be found in the literature, there is a notable lack of data on alternative pumping methods and their advantages and disadvantages compared with the traditional pump diodes emitting at the 793 nm wavelength. This work aims to complement this missing knowledge by providing a comprehensive theoretical and experimental comparison of three different pumping schemes.

2. Numerical Model

In essence, fiber lasers consist of a cavity formed by enclosing rare-earth-doped fiber, known as the active fiber, between two mirrors, typically implemented by using Fiber Bragg Gratings (FBGs) [25]. One of these mirrors has extremely high reflectivity, typically >99%, while the output coupler (OC) mirror has significantly lower reflectivity, typically between 4 and 10%. The pump, which is commonly generated with semiconductor laser diodes, is coupled to the active fiber by using special pump combiners [26]. The modeling of fiber lasers requires the simultaneous solving of a set of rate equations, which describe the evolution of populations at the various energy levels, and of propagation equations for the pump and laser waves. The energy-level scheme for Tm^{3+} ions in a silica host is reported in Figure 1.

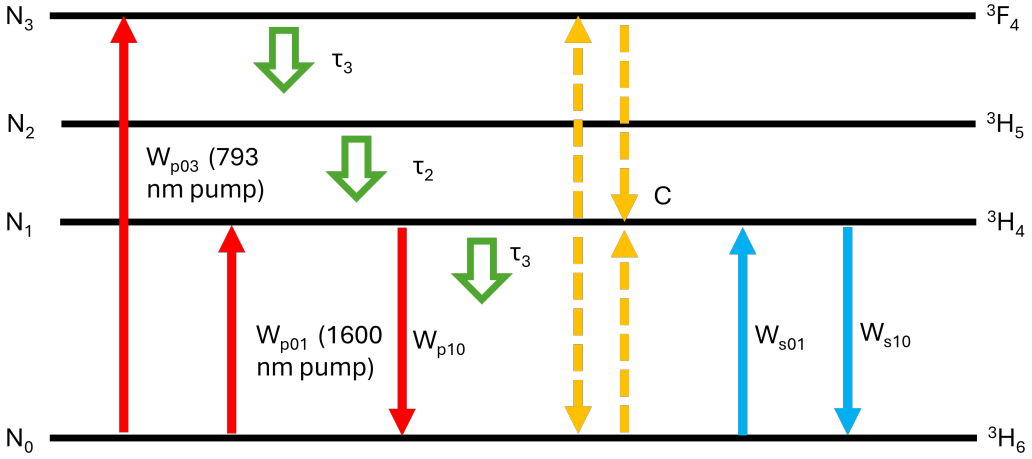

Figure 1. Energy diagram of thulium ions in a silica host. The meaning of the various symbols is described in the text.

The out-of-band pumping scheme uses photons at a wavelength of 793 nm, generated by a GaAs-based laser diode, to promote ions from the ground state $^3H_6$ to the excited energy level $^3F_4$. From this upper level, the excited ions rapidly decay, without emitting radiation, to the $^3H_4$ level, characterized by a longer lifetime, before ultimately returning to the ground state through photon- and phonon-assisted transitions. The efficiency of this process can be enhanced by a cross-relaxation mechanism (denoted by "C" in Figure 1) in which the decay of an ion from $^3F_4$ to level $^3H_4$ transfers energy to another thulium ion, exciting it from ground state $^3H_6$ to the $^3H_4$ level. As a result, two ions were excited to level $^3H_4$ with one 793 nm photon, from which they eventually jump back to the ground state, generating two laser photons via stimulated emission [27].

For out-of-band pumping, the three key energy levels involved in the laser transition correspond to the populations labeled N_0, N_1, and N_3 in Figure 1. It is, therefore, possible to write the following set of time-dependent rate equations:

$$\frac{dN_3(z,t)}{dt} = w_{p,03} - \frac{N_3(z,t)}{\tau_3} - C \tag{1}$$

$$\frac{dN_1(z,t)}{dt} = -w_{s,10} + w_{s,01} - \frac{N_1(z,t)}{\tau_1} + \frac{\beta_{31}N_3(z,t)}{\tau_3} + 2C \tag{2}$$

$$N_0(z,t) = -N_T - N_1(z,t) - N_3(z,t), \tag{3}$$

where w_{ij} is the transition rate from level i to j and represents the probability of stimulated emission (or absorption) between energy levels i and j; N_T is the total density of Tm ions; τ_1 and τ_3 refer to the spontaneous lifetime of levels $^3H_4$ and $^3F_4$, respectively; and β_{31} is the

branching ratio of the spontaneous transition from level 3 to 1. Cross-relaxation processes are taken into account in the term C, which can be expressed as

$$C = k_{3101}\, N_0(z,t)\, N_3(z,t) - k_{1310}\, N_1^2(z,t), \tag{4}$$

where k_{3101} and k_{1301} are the cross-relaxation constants between the three energy levels involved. The transition rates w_{ij} are related to the optical intensity I and photon energy $h\nu$ through the transition cross-section σ as

$$w_{\mathrm{ij}} = \sigma_{\mathrm{ij}} \frac{I}{h\nu}. \tag{5}$$

This way, the transition rate $w_{\mathrm{p},03}$ is proportional to the pump intensity I_{p} at frequency ν_{p} through the pump absorption cross-section $\sigma_{\mathrm{p}}^{\mathrm{a}}$. Similarly, the transition rates $w_{\mathrm{s},10}$ and $w_{\mathrm{s},01}$ are proportional to the signal intensity I_{s} at frequency ν_{s} through the signal emission cross-section $\sigma_{\mathrm{s}}^{\mathrm{e}}$ and the signal absorption cross-section $\sigma_{\mathrm{s}}^{\mathrm{a}}$, respectively.

In contrast, in the in-band pumping scheme, the Tm^{3+} ions are excited from the ground state to an excited energy level via the absorption of pump photons in the L-band. From this excited energy level, the Tm^{3+} ions rapidly decay via non-radiative processes to the $^3H_4$ energy level. The rate equations describing the population densities are

$$\frac{\mathrm{d}N_3(z,t)}{\mathrm{d}t} = -\frac{N_3(z,t)}{\tau_3} - C \tag{6}$$

$$\frac{\mathrm{d}N_1(z,t)}{\mathrm{d}t} = -w_{\mathrm{s},10} + w_{\mathrm{s},01} - \frac{N_1(z,t)}{\tau_1} + \frac{\beta_{31} N_3(z,t)}{\tau_3} + 2C - w_{\mathrm{p},10} + w_{\mathrm{p},01}, \tag{7}$$

plus Equation (3), which describes the conservation of Tm^{3+} ions in the fiber and is therefore the same for both pumping schemes.

By using pump photons with longer wavelength and lower energy, the population density N_3 relative to energy level $^3F_4$ is expected to be very low, since it is no more involved in the energy exchange processes. Since we cannot say that this value is zero rather than very small, the cross-relaxation term C is nonetheless included in the rate equations, as it can still influence the overall dynamics of the system.

Given the dependency of the transition rates on the pump and signal intensities, the rate equations must be coupled with pump and signal propagation equations. For out-of-band and in-band tandem pumping, assuming a single-pass pump, only three propagation equations must be considered: pump intensity P at either 793 nm or at 1600 nm, and forward- and backward-propagating signals $S^{\pm}$ at the lasing wavelength:

$$\begin{cases} \dfrac{\mathrm{d}\,P}{\mathrm{d}\,z} = \left[\Gamma_{\mathrm{p}}\sigma_{\mathrm{p}}^{\mathrm{e}}\, N_3 - \Gamma_{\mathrm{p}}\sigma_{\mathrm{p}}^{\mathrm{a}}\, N_1 - \alpha_{\mathrm{p}}(\lambda_{\mathrm{p}})\right] P \\ \dfrac{\mathrm{d}\,S^{\pm}}{\mathrm{d}\,z} = \pm[\Gamma_s\sigma_e^e N_1 - \Gamma_{\mathrm{s}}\sigma_{\mathrm{s}}^{\mathrm{a}}\, N_0 - \alpha_{\mathrm{s}}(\lambda_{\mathrm{s}})]\, S^{\pm} \end{cases}, \tag{8}$$

where $\Gamma_{\mathrm{p}} = 0.0064$ and $\Gamma_{\mathrm{s}} = 0.77$ are the pump and signal confinement factors, respectively, and $\alpha_{\mathrm{p}}(\lambda_{\mathrm{p}})$ and $\alpha_{\mathrm{s}}(\lambda_{\mathrm{s}})$ are the pump and signal propagation losses, at the respective wavelengths. As for the boundary conditions,

$$\begin{cases} P(0) = P_{\mathrm{C}} \\ S^{+}(0) = R_{\mathrm{HR}}(\lambda_{\mathrm{s}})\, S^{-}(0) \\ S^{-}(L) = R_{\mathrm{OC}}(\lambda_{\mathrm{s}})\, S^{+}(L) \end{cases}, \tag{9}$$

where P_C is the coupled pump power, R_{HR} is the reflectivity of the high-reflectivity mirror, R_{OC} is the reflectivity of the output coupler, and L is the active fiber length.

The intracavity pumping scheme is somewhat more complex. In this approach, a pump generated by semiconductor lasers at any wavelength within the 915-to-976 nm range is absorbed by the Er/Yb-doped fiber while passing through the Tm-doped fiber with minimal attenuation. Meanwhile, the emitted signal by the Er/Yb-doped fiber close to 1600 nm is absorbed by the Tm-doped fiber, where it excites the ions, ultimately leading to emission in the 1900-to-2000 nm range. A schematic representation of this configuration is shown in Figure 2. This approach has already demonstrated its effectiveness in enhancing efficiency in solid-state lasers based on crystal hosts [28–30], though its application in fiber lasers has been less extensively documented [31].

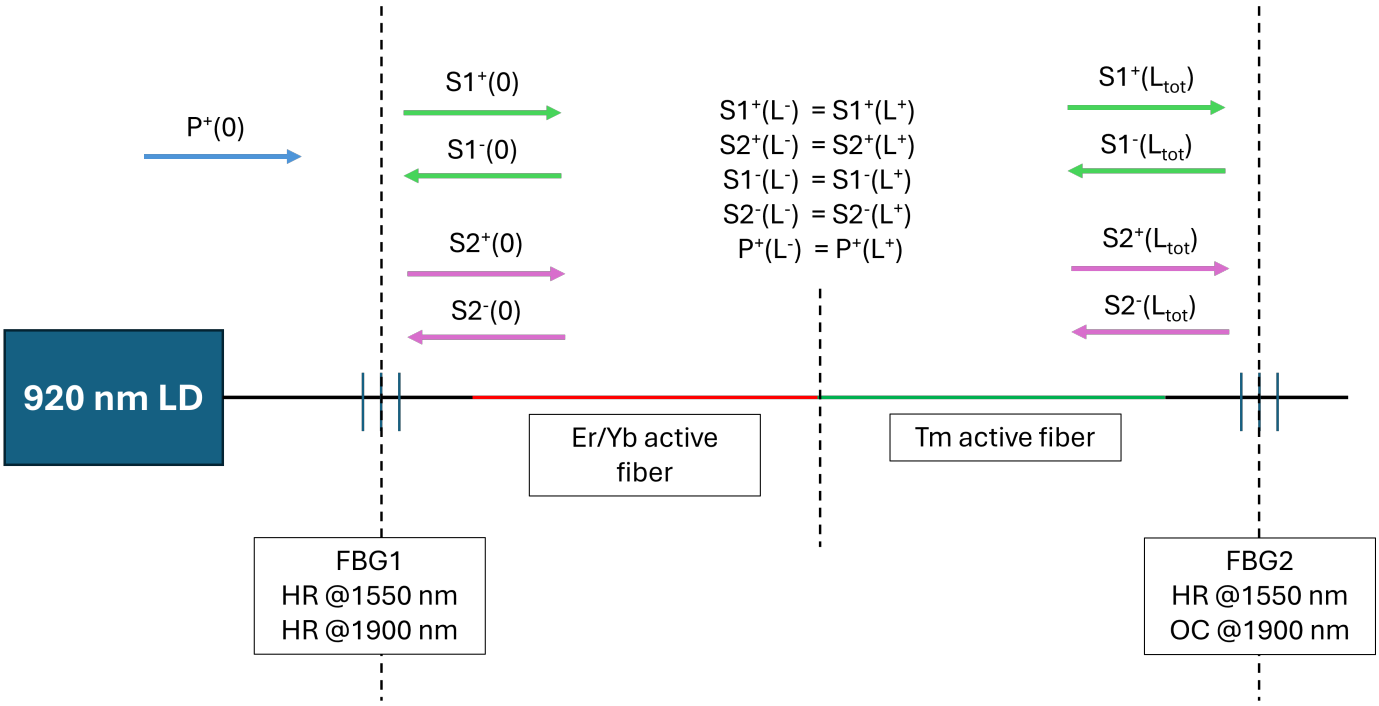

Figure 2. Scheme of an intracavity pumped Tm-doped fiber laser. In the scheme, P refers to the pump power coming from the multiemitter module, S1 refers to the laser signal centered at 1550 nm, and S2 refers to the laser signal centered at 1900 nm.

In this case, the two mirrors confining the cavity must have a special spectral profile. Indeed, they need to be transparent at the wavelength used to pump the Er/Yb-doped fiber (assuming, again, a single-pass pump) while exhibiting high reflectivity around 1600 nm. Additionally, one mirror must have high reflectivity at the Tm emission wavelength, while the other must have partial reflectivity at this wavelength. These complex spectral responses can be precisely engineered through the direct inscription of the FBGs using a femtosecond laser, employing either Point-by-Point or Line-by-Line fabrication methods [32–34].

In the experimental setup analyzed in this work, a 915 nm semiconductor laser was selected as the pump source (K915FG1RN-110.0W) for the Er/Yb-doped fiber laser. This choice enhances the system's robustness, as relying on the alternative higher-absorption cross-section of Yb at 976 nm would make the overall efficiency much more sensitive to small fluctuations in the laser module's emission wavelength. Furthermore, the Tm-doped portion of the laser was pumped at 1550 nm instead of the more optimal 1600 nm. This decision helps mitigate the risk of Catastrophic Optical Damage (COD) in the Er/Yb fiber caused by Amplified Spontaneous Emission (ASE) phenomena, thereby improving the overall stability and robustness of the system. In fact, in Er/Yb fiber lasers, achieving a

signal output centered at 1600 nm is not straightforward due to the potential occurrence of ASE phenomena, which in Er/Yb active fibers are typically centered at 1550 nm. To prevent ASE, which is one of the physical phenomena leading to COD, it is crucial to minimize losses within the Er/Yb cavity. However, in an intracavity laser like the one described in this article, the Tm active fiber itself introduces internal losses within the Er/Yb cavity. The risk of ASE phenomena increases as the signal emission wavelength moves farther from 1550 nm, so using this wavelength guarantees a system that is more robust to optical losses. As will be explained later in this article, non-negligible splice losses also contribute to the susceptibility to ASE-related phenomena in the laser cavity. The propagation equations are five equations, similar to those in Equations (8), one for the pump provided by the semiconductor laser and two (forward and backward propagating) for each of the signals, S_1 at 1500 nm and S_2 at 1900 nm. Particular attention must be paid to the boundary conditions. With reference to Figure 2, we have

$$\begin{cases} P(0) = P_C \\ S_1^+(0) = R_{HR}(\lambda_{s1})\, S_1^-(0) \\ S_1^-(L_1 + L_2) = R_{OC}(\lambda_{s1})\, S_1^+(L_1 + L2) \\ S_2^+(0) = R_{HR}(\lambda_{s2})\, S_2^-(0) \\ S_2^-(L_1 + L_2) = R_{OC}(\lambda_{s2})\, S_2^+(L_1 + L2) \end{cases}, \tag{10}$$

where $\lambda_{s1} = 1550$ nm and $\lambda_{s2} = 1900$ nm, $R_{HR}(\lambda_{s1}) \simeq R_{HR}(\lambda_{s2}) \simeq R_{OC}(\lambda_{s1}) \simeq 99\%$, and $R_{OC}(\lambda_{s2}) \simeq 4 - 10\%$. Additionally, continuity conditions must be enforced at the junction between the two active fibers.

The mathematical framework briefly described here was simulated by using a custom-developed algorithm in Matlab® R2024a [35], while the separate in-band and out-of-band systems were modeled by using RP Fiber Power® [36]. Notably, RP Fiber Power includes a mode-solver feature for analyzing mode distribution within the fiber and offers a wide range of configurable parameters for both input signals and pump beams. These parameters include input power, wavelength, radial intensity profile, losses, and propagation direction. This flexibility makes RP Fiber Power particularly well -suited for our theoretical analysis, providing both ease of use and robust simulation capabilities.

3. Results

3.1. Theoretical Comparison

To theoretically compare the efficiency of the three different pumping schemes, the parameters of the active fiber were derived from literature data [37]. A summary of these values is provided in Table 1.

Intrinsic losses at signal and pump wavelengths were assumed to be negligible. Similarly, the splices were assumed to be ideal and therefore lossless. The Tm-doped active fiber was assumed to be a double-clad fiber (DCF) with a 10 µm core diameter and a 130 µm cladding diameter, with unidirectional pumping by a 793 nm laser diode coupled to the inner cladding of the TFL. Since high-power laser diodes are highly multi-mode, the pump distribution is considered to be a circular flat-top beam with radius equal to that of the inner cladding of the fiber. The signal is instead single-mode, so it is assumed to have a Gaussian distribution with beam diameter equal to the Mode Field Diameter (MFD).

Table 1. Parameters of the active fiber for the analysis of the two Tm-doped fiber laser configurations [37].

Parameter	Value
τ_1	540 µs
τ_3	14.2 µs
σ_p^a (793 nm)	5×10^{-25} m^2
σ_s^e	5×10^{-25} m^2
σ_s^a	1×10^{-26} m^2
C	3×10^{-23} m^{3}s^{-1}
β_{31}	0.72
N	1.46×10^{26} m^{-3}

Different lengths of the active fiber were considered, ranging from 10 m to 18 m; the results are reported in Figure 3. As can be observed, the influence of active fiber length on the efficiency of TFL is poor in the pump power range of interest. This is due to the fact that in the first approximation, for the amount of pump power here analyzed, the absorption exhibits an exponential trend with respect to the fiber length; therefore, the difference in terms of power absorption is minimal. At the same time, the simulations considered a small, nearly negligible signal re-absorption coefficient; therefore, the impact of the fiber length on the efficiency of the FL is poor.

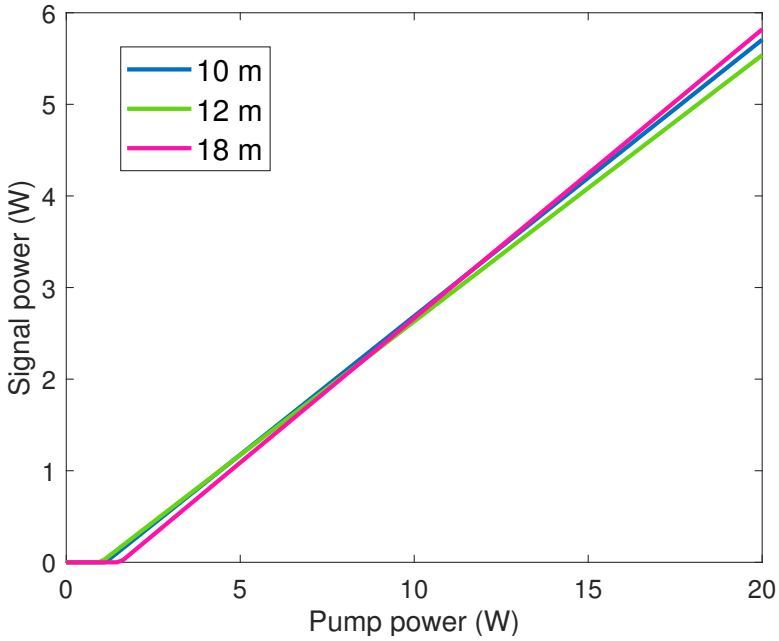

Figure 3. Output power of the indirect pumped TFL for different active fiber lengths, considering a maximum pump power of 20 W and R_{HR} = 99% and R_{OC} = 10%.

In the second case of this comparison, i.e., using the Er/Yb fiber laser emission at 1600 nm, it is possible to have a nearly single-mode pump that can thus be coupled to the core of the Tm-doped fiber. Therefore, in this case, the pump can also be modeled as a Gaussian beam whose diameter is the MFD. As before, different fiber lengths were studied and the effects of the different fiber length on the fiber efficiency are reported in Figure 4.

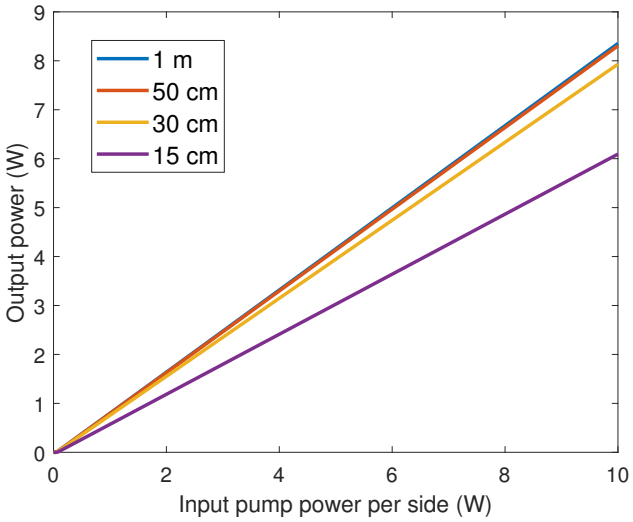

Figure 4. Output power of the in-band-pumped TFL for different active fiber lengths and assuming a maximum pump power of 10 W, R_{HR} = 99%, and R_{OC} = 10%.

As can be observed in Figure 4, the lengths of active fiber considered for this alternative L-band pumping scheme are much shorter than those considered for the out-of-band pumping scheme, approximately two orders of magnitude shorter. This aspect, in combination with the much higher slope efficiency observed with the L-band pump source (80%, versus the 30% predicted for the out-of-band pumping scheme) makes the in-band pumping scheme interesting in terms of cost reduction, higher quantum efficiency, and consequently, lower thermal power to be handled. The increase in efficiency is also evident in the very low value of threshold pump power, as seen in Figure 4. Furthermore, from the experimental point of view, since the threshold pump power has a much lower value than the minimum output power generated by the developed Er/Yb laser source, this aspect was not further investigated since there was no possibility of validating the simulation results with experiments.

Different values of the output coupler (OC) reflectivity were simulated, keeping the fiber length constant at 15 cm. The comparison for these three cases is reported in Figure 5.

In the simulation of the intracavity pumping scheme, many different combinations in terms of fiber length (both of the Er/Yb and of the Tm portions) and OC Fiber Bragg Grating (FBG) reflectivity values were considered; the most interesting ones are reported in Figure 6.

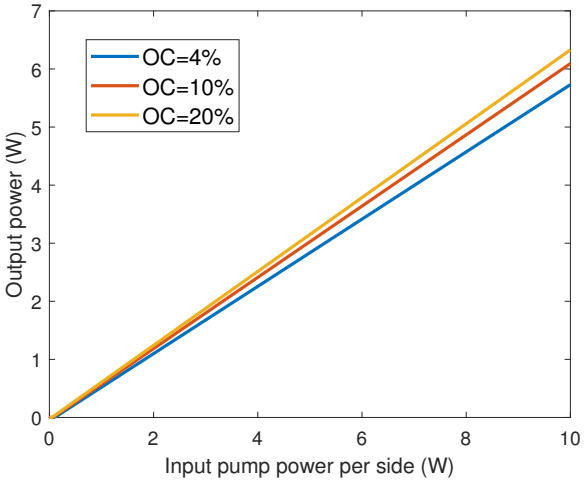

Figure 5. Output power of the in-band-pumped TFL for different OC reflectivity values and assuming maximum pump power 10 W, R_{HR} = 99%, and fiber length 15 cm.

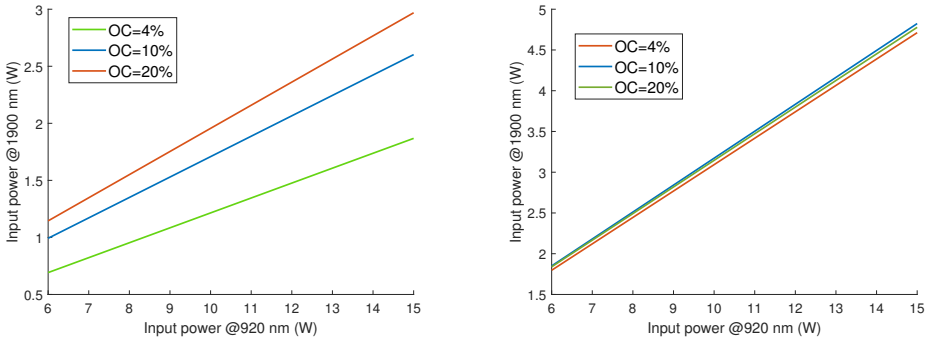

Figure 6. Comparison of the efficiency for different OC reflectivity values considering two different Tm active fiber lengths. In particular, (**a**) L_{Tm} = 50 cm and (**b**) L_{Tm} = 1 m

It appears evident from the simulations that there is no significant improvement when using an intracavity configuration, even in the best-case scenario (in particular, of negligible loss due to splices); in fact, the efficiency values resulting from the simulation analysis are comparable to those obtained from the results of the out-of-band and in-band pumping schemes. However, since the purpose of this discussion is also to analyze the impact of experimental non-idealities on the three different configurations, an experimental analysis was carried out.

3.2. Experimental Analysis

The simulation results described in the previous section were experimentally demonstrated by assembling a high-efficiency, in-band-pumped fiber laser using an ad hoc developed 1600 nm fiber laser as the pump source. The scheme of the fiber laser is shown in Figure 7.

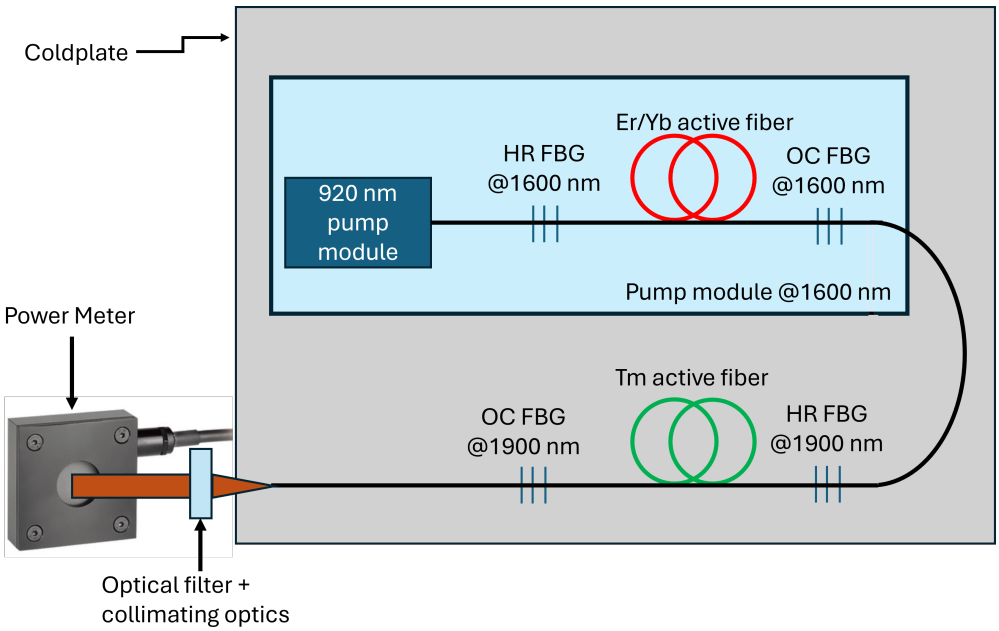

Figure 7. Experimental setup for the in-band-pumped Tm-doped fiber laser emitting at 1900 nm.

The output power was measured with apower meter from Thorlabs Inc. (Newton, NJ, USA), and signal power was separated from any residual pump signal by using a wide-band band-pass filter, FB1900-200 from Thorlabs Inc. (Newton, NJ, USA). During the experimental work, particular care was taken to minimize the impact of experimental non-idealities, for example, maintaining a constant beam size on the power meter throughout

the measurements, eliminating potential uncertainties arising from beam dimension irregularities. Prior to the experiments, the power meter was calibrated, and all environmental conditions—particularly ambient temperature and sensor temperature—were carefully monitored and controlled. Despite thorough efforts to minimize uncertainty sources, some factors could not be entirely mitigated, such as the angular dependence of the power meter and the fiber cleave angle. Taking into account all identified sources of uncertainty, the overall RMS noise of the power measurement is approximately 7%. The output spectrum was acquired by sampling the back-reflections coming from the power meter by using a NIRQuest+2.2 spectrometer by OceanOptics (Orlando, FL, USA), featuring a wavelength range spanning from 900 to 2120 nm and an optical resolution of 4.8 nm.

In order to find the configuration with the highest associated efficiency, different fiber lengths and different OC reflectivity values were experimentally investigated. As a result, the optical–optical efficiency was found to be about 50%, lower than the approximately 75% observed in other experimentally validated in-band-pumped laser cavities reported in the literature [38,39]. An explanation for this discrepancy can be found in the non-ideal behavior of the components. For example, in the simulations presented in the previous section, the splices were assumed to be ideal, while in the experiments, splice losses had an average value of 10% due to the splicers used in these experimental activities. The effect of the non-negligible splice losses on the overall efficiency of the laser can be observed in Figure 8.

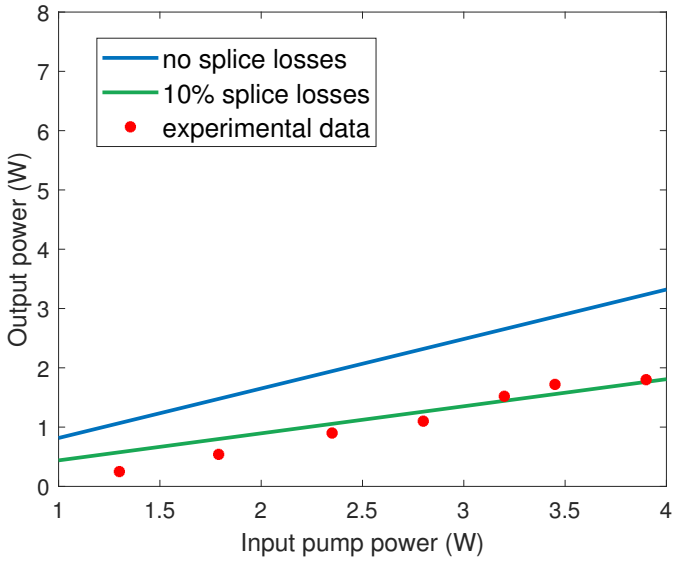

Figure 8. Comparison among experimental data, simulation data considering negligible splice losses, and simulation data considering 10% splice losses.

Moreover, while all simulations considered a negligible contribution of ASE, with the experimental analysis, this assumption was proved incorrect. In fact, for fibers longer than 50 cm, the OC should be higher than the Fresnel reflection (i.e., broadband OC reflectivity of 4%) to avoid the detrimental contribution of ASE by generating a stronger laser signal which is not competing with the unwanted spontaneous emission at other wavelengths. Therefore, to achieve stable signal emission without the risk of COD, some form of mitigation for ASE needs to be implemented. This can be performed by either suppressing losses, as previously described for the intracavity configuration, or increasing the signal power maintained inside the cavity (in other words, increasing the OC reflectivity). However, there is no possibility of addressing these cavity losses since their main contribution is represented by splice-related losses, which are inevitable with the equipment available to us. Consequently, with

the experimental analysis, it was shown that higher OC reflectivities lead to more robust laser operation while also leading to a lower overall efficiency.

It should also be highlighted that the 1600 nm pump implemented with the Er/Yb fiber laser allows for the use of a core-pumped configuration, which is very interesting, as it enables to have an extremely high overlap between the pump power and the doped area. In numbers, in a core-pumped configuration, this overlap is greater than 85%, while this value drops to less than 1% for a cladding-pumped system.

In the set of graphs in Figures 9–11, it is possible to observe the best experimental results for different fiber lengths. It is impressive to note that significant values of output power compatible with biomedical applications can be reached with only 10 cm of active fiber [40]. Optical–optical efficiency is also high, reaching 55.5%.

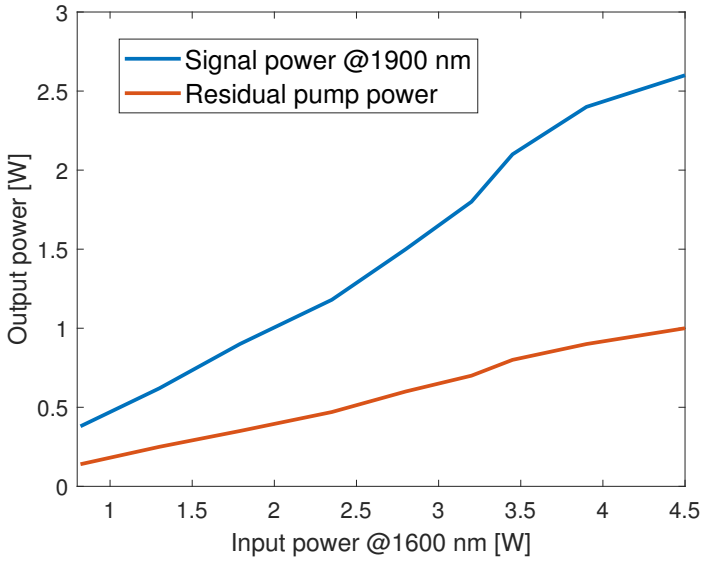

Figure 9. Laser signal power and residual pump power at 1600 nm of a TFL emitting at 1900 in core-pumped configuration with L = 20 cm and OC = 3 dB.

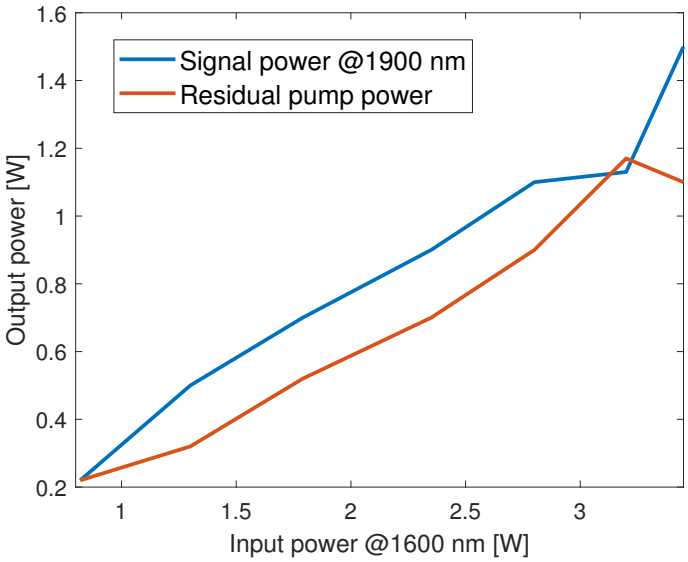

Figure 10. Laser signal power and residual pump power at 1600 nm of a TFL emitting at 1900 in core-pumped configuration with L = 10 cm and OC=Fresnel reflection.

In the intracavity configuration, the pump source was a multiemitter source, centered at 915 nm with a maximum output power of 110 W from BWT (Beijing, China) (K915FG1RN-110.0W). The Tm-doped active fiber employed was SM-TDF-10P/130-M by Coherent

(Saxonburg, PA, USA), while the Er/Yb active fiber was MM-EYDF-10/125-XP, also by Coherent. These are the same fibers employed in both the L-band laser source and the in-band-pumped Tm fiber laser previously described. The intracavity configuration uses two high-reflectivity (HR) FBGs centered at 1550 nm. Using this wavelength, instead of 1600 nm, makes the system more robust to ASE effects, at the expense of the efficiency in pumping the Tm-doped fiber. The output spectrum was acquired by using a spectrometer by OceanOptics (NIRQuest+2.2), while the output power and its different contributions were measured with a power meter by Thorlabs, selecting the different wavelengths by using two band-pass filters (FB1900-200 and FELH-0950 by Thorlabs Inc. (Newton, NJ, USA)).

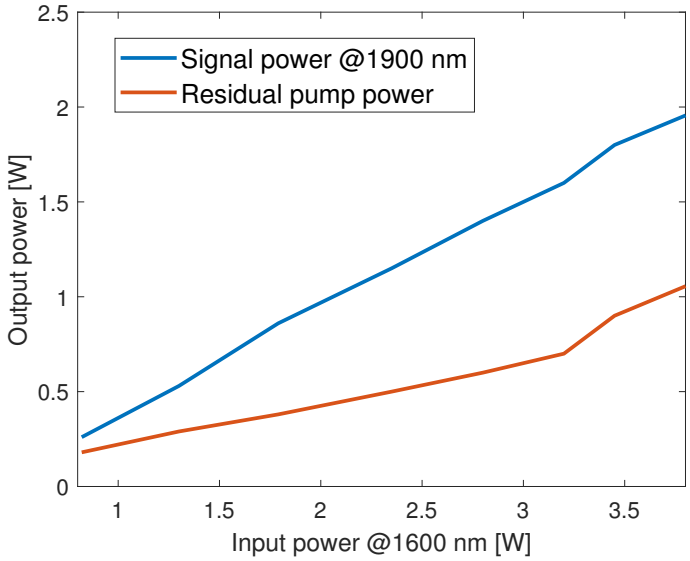

Figure 11. Laser signal power and residual pump power at 1600 nm of a TFL emitting at 1900 in core-pumped configuration with L = 15 cm and OC = 1.5 dB.

The Er/Yb active fiber length was kept fixed at 5.2 m in all the experiments. This length was chosen in order to ensure that the amount of input pump power absorbed by the cavity is higher than 95%. The parameters that were varied are the Tm-doped active fiber length and the OC mirror reflectivity. The results are reported in Figure 12.

As can be observed in Figure 12, the laser efficiency is poorly affected by the active fiber length or the OC reflectivity, at least with the power levels analyzed in this work. This is in partial accordance with the simulation results. The significant drop in optical–optical conversion efficiency may be partially attributed to splice losses, as their average contribution was measured to be in the order of 10%. It is evident that the average splice loss in our experimental analysis is far higher than the state of the art, which is approximately 0.23%. However, the splices considered in the experimental analysis were performed with a small, non-programmable FSM-40S splicer from Fujikura (Tokyo, Japan), whose lack of programmability prevented improving the splice losses and scaling up the power. Nevertheless, the purpose of the work described in this article was to compare different pumping methods; therefore, in the experimental activities, the significant splice losses were simply taken into account. In fact, a statistical analysis was performed on splice losses by repeating the splicing procedures 30 times. The result was an average loss of 10% ± 3%. For the intracavity scheme in particular, since all splices are inside the laser cavity, their impact on the output power is enhanced. Also, the difference between the simulation results and the experimental results can be partially attributed to the mismatch between the core of the two active fibers. This aspect was not considered in the simulations. This

deviation from the simulations can be observed from the comparison of the set of curves in Figure 12 and the set of curves in Figure 6.

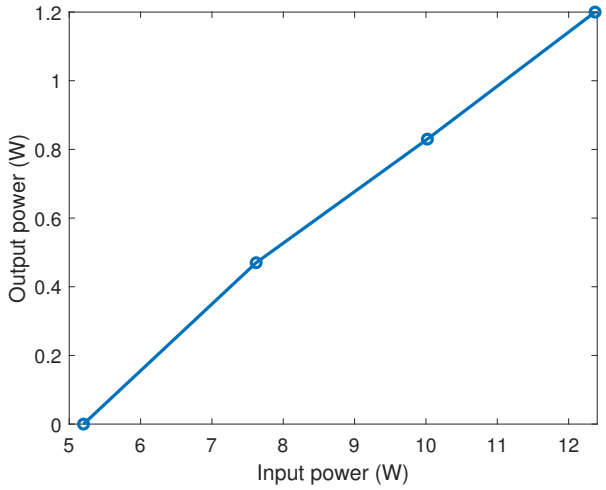

(**a**)

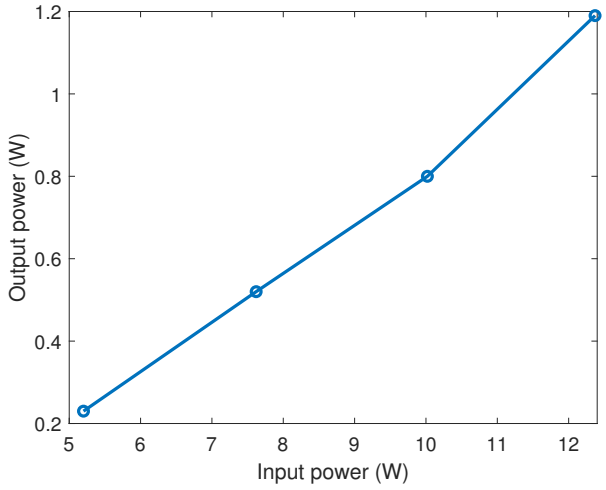

(**b**)

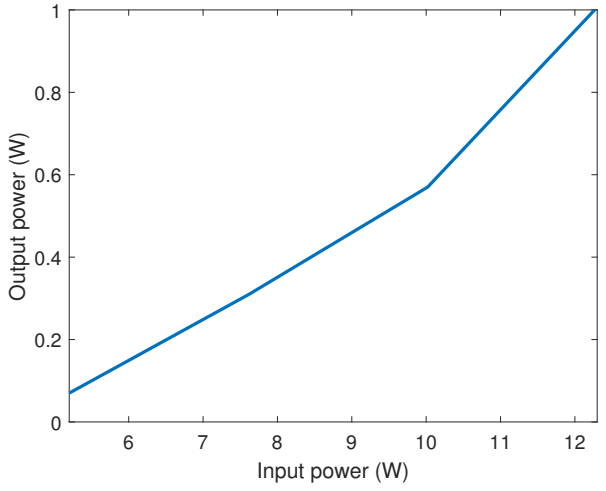

(**c**)

Figure 12. Laser signal power optimized for three different active fiber lengths, in particular (**a**) L_{Tm} = 1 m and OC = 31%, (**b**) L_{Tm} = 0.5 m and OC = 64.5%, and (**c**) L_{Tm} = 1.2 m and OC = 4%.

The experimental analysis highlighted the susceptibility of the structure to variations in the Tm active fiber length. In fact, with shorter portions of fiber, the experimental result was a fiber fuse due to an excess of power density in the fiber. On the other hand, increasing the length of the Tm active fiber implies the onset of ASE phenomena, which deteriorates the laser signal.

4. Discussion

At first glance, the in-band tandem pumped configuration may seem like the ideal solution for a high-power Tm-doped fiber laser at 1900 nm wavelength. In fact, the efficiency of the in-band scheme resulted to be much higher (theoretically 75%, experimentally demonstrated 50%) than the traditional out-of-band scheme. Moreover, the length of Tm-doped active fiber needed is nearly two orders of magnitude smaller. However, there are other considerations to be taken into account:

- The improvement in the efficiency of the TFL was achieved at the expense of the addition of the Er/Yb laser. When working with a tandem configuration, the overall efficiency of the system needs to consider the efficiency of both stages. Experimentally, it was observed that the overall efficiency of the FL is lower than 40% and therefore comparable with the results reported for the traditional out-of-band pumping scheme.
- The addition of two extra splices in the system may affect its long-term reliability.
- Even if the strong reduction in the length of the Tm active fiber may reduce the cost of the device, the small length of active fiber needed for surgical application makes the system prone to unwanted effects; in fact, small changes in active fiber length strongly affect the efficiency of the laser.

Taking these aspects into account, a configuration of this sort would not be of interest for surgical applications. The significant decrease in active fiber length may have a positive impact for high-power fiber lasers employed for material processing. However, to conduct a study of this kind, it is necessary to develop a 1600 nm source of adequate power.

For what concerns the intracavity configuration, it is also subject to experimental unwanted phenomena such as splice losses, which strongly affect the overall laser performance. Moreover, the onset of parasitic lasing is facilitated by the insertion of a high-loss element in the cavity, represented by the Tm-doped fiber. Therefore, for the experimental maturity and setup available at the moment, the intracavity laser has been ruled out for its use in surgical applications.

5. Conclusions

The article presented here provides a theoretical and experimental analysis of three different pumping methods for a Tm-doped fiber laser, with a particular focus on lasers for surgical applications. The theoretical comparison has already highlighted that intracavity pumping does not offer significant practical advantages over out-of-band and in-band pumping. The experimental investigation has further demonstrated the practical limitations of configurations other than out-of-band pumping in terms of reliability and repeatability, ruling out the use of alternative pumping methods, at least for CW thulium fiber lasers for surgical applications.

The research study presented here highlights the potential of the use of a tandem in-band pumping scheme for industrial applications and Q-switched pulsed lasers. The authors are currently conducting further studies to explore this aspect in greater depth.

Author Contributions: Conceptualization, V.S. and G.P.; Methodology, A.M., M.C., S.Z. and J.M.B.T.; Validation, L.M.T.; Investigation, C.B.P.; Writing—original draft, V.S.; Writing—review & editing, A.M., C.B.P. and G.P.; Supervision, G.M.; Project administration, G.P. All authors have read and agreed to the published version of the manuscript.

Funding: This research study received no external funding.

Institutional Review Board Statement: Not applicable.

Data Availability Statement: Data are contained within the article.

Conflicts of Interest: Authors Luca Maggio Tanasi, Sabina Zaimovic, José Maria Blanco Triana and Gabriella Motta were employed by the company Alite S.r.l. The remaining authors declare that the research was conducted in the absence of any commercial or financial relationships that could be construed as a potential conflict of interest.

Abbreviations

The following abbreviations are used in this manuscript:

FL	fiber laser
TFL	thulium fiber laser
DCF	double-clad fiber
COD	Catastrophic Optical Damage
ASE	Amplified Spontaneous Emission
OC	output coupler
HR	high reflectivity
MFD	Mode Field Diameter

References

1. Shi, W.; Fang, Q.; Zhu, X.; Norwood, R.A.; Peyghambarian, N. Fiber lasers and their applications. *Appl. Opt.* **2014**, *53*, 6554–6568. [PubMed]
2. Zervas, M.N.; Codemard, C.A. High Power Fiber Lasers: A Review. *IEEE J. Sel. Top. Quantum Electron.* **2014**, *20*, 219–241.
3. Richardson, D.J.; Nilsson, J.; Clarkson, W.A. High power fiber lasers: Current status and future perspectives. *J. Opt. Soc. Am. B* **2010**, *27*, B63–B92. [CrossRef]
4. Jeong, Y.; Boyland, A.J.; Sahu, J.K.; Chung, S.; Nilsson, J.; Payne, D.N. Multi-kilowatt Single-mode Ytterbium-doped Large-core Fiber Laser. *J. Opt. Soc. Korea* **2009**, *13*, 416–422.
5. Wang, Y.; Kitahara, R.; Kiyoyama, W.; Shirakura, Y.; Kurihara, T.; Nakanish, Y.; Yamamoto, T.; Nakayama, M.; Ikoma, S.; Shima, K. 8-kW single-stage all-fiber Yb-doped fiber laser with a BPP of 0.50 mm-mrad. In Proceedings of the Fiber Lasers XVII: Technology and Systems, SPIE LASE, San Francisco, CA, USA, 21 February 2020; International Society for Optics and Photonics (SPIE): Washington, DC, USA, 2020; Volume 11260, p. 1126022.
6. Lin, W.; Desjardins-Carrière, M.; Iezzi, V.L.; Vincelette, A.; Bussières-Hersir, M.H.; Rochette, M. Simple design of Yb-doped fiber laser with an output power of 2 kW. *Opt. Laser Technol.* **2022**, *156*, 108448.
7. Bremer, K.; Pal, A.; Yao, S.; Lewis, E.; Sen, R.; Sun, T.; Grattan, K.T.V. Sensitive detection of CO_2 implementing tunable thulium-doped all-fiber laser. *Appl. Opt.* **2013**, *52*, 3957–3963. [CrossRef]
8. Pal, A. Thulium-Doped Fibre Laser in the 2 µm Wavelength Region for Gas Sensing. Unpublished Ph.D. Thesis, City University London, London, UK, 2013.
9. Jones, P.; Beisland, C.; Ulvik, Ø. Current status of thulium fibre laser lithotripsy: An up-to-date review. *BJU Int.* **2021**, *128*, 531–538.
10. Fried, N.M. Thulium fiber laser lithotripsy: An in vitro analysis of stone fragmentation using a modulated 110-watt Thulium fiber laser at 1.94 µm. *Lasers Surg. Med.* **2005**, *37*, 53–58. [CrossRef]
11. Blackmon, R.L.; Irby, P.B.; Fried, N.M. Thulium fiber laser lithotripsy using tapered fibers. *Lasers Surg. Med.* **2010**, *42*, 45–50. [CrossRef]
12. Ulvik, Ø.; Æsøy M.S.; Juliebø-Jones, P.; Gjengstø, P.; Beisland, C. Thulium Fibre Laser versus Holmium:YAG for Ureteroscopic Lithotripsy: Outcomes from a Prospective Randomised Clinical Trial. *Eur. Urol.* **2022**, *82*, 73–79. [CrossRef]
13. Uleri, A.; Farré, A.; Izquierdo, P.; Angerri, O.; Kanashiro, A.; Balaña, J.; Gauhar, V.; Castellani, D.; Sanchez-Martin, F.; Monga, M.; et al. Thulium Fiber Laser Versus Holmium:Yttrium Aluminum Garnet for Lithotripsy: A Systematic Review and Meta-analysis. *Eur. Urol.* **2024**, *85*, 529–540. [CrossRef] [PubMed]
14. Mingareev, I. Welding of polymers using a 2 µm thulium fiber laser. *Opt. Laser Technol.* **2012**, *44*, 2095–2099.

15. Böhm, S.; Schmidt, M.; Stichel, T.; Kahlmeyer, M.; Kryukov, I.; Sommer, N. Single-step Laser Plastic Deposition (LPD) using a near-infrared Thulium fiber-laser. *Polym. Test.* **2020**, *81*, 106185. [CrossRef]
16. Engin, D.; Mathason, B.; Storm, M. Efficient, space-based, PM 100W thulium fiber laser for pumping Q-switched 2um Ho:YLF for global winds and carbon dioxide lidar. In Proceedings of the Lidar Remote Sensing for Environmental Monitoring 2017, San Francisco, CA, USA, 8–9 August 2017; International Society for Optics and Photonics (SPIE): Washington, DC, USA, 2017; Volume 10406, p. 104060B.
17. Currey, R.; Khademian, A.; Shiner, D. Development of a Thulium Fiber Laser for an Atomic Spectroscopy Experiment. *Fibers* **2020**, *8*, 12. [CrossRef]
18. Sincore, A.; Bradford, J.D.; Cook, J.; Shah, L.; Richardson, M.C. High Average Power Thulium-Doped Silica Fiber Lasers: Review of Systems and Concepts. *IEEE J. Sel. Top. Quantum Electron.* **2018**, *24*, 0901808.
19. Baravets, Y.; Todorov, F.; Honzatko, P. High-power thulium-doped fiber laser in an all-fiber configuration. In Proceedings of the 20th Slovak-Czech-Polish Optical Conference on Wave and Quantum Aspects of Contemporary Optics, Jasna, Slovakia, 5–9 September 2016; Müllerová, J., Senderáková, D., Ladányi, L., Ľubomír, S., Eds.; International Society for Optics and Photonics (SPIE): Washington, DC, USA, 2016; Volume 10142, p. 101420G.
20. Lukasz, S.; Lukasz, P.; Samir, L.; Mark, F.; Benson, T.M.; Seddon, A.B.; Slawomir, S. Experimental Investigation of Actively Q-Switched Er3+:ZBLAN Fiber Laser Operating at around 2.8 µm. *Sensors* **2020**, *20*, 4642. [CrossRef]
21. Guillemot, L.; Loiko, P.; Doualan, J.L.; Braud, A.; Camy, P. Excited-state absorption in thulium-doped materials in the near-infrared. *Opt. Express* **2022**, *30*, 31669–31684.
22. Daniel, J.M.O.; Simakov, N.; Tokurakawa, M.; Ibsen, M.; Clarkson, W.A. Ultra-short wavelength operation of a thulium fibre laser in the 1660–1750 nm wavelength band. *Opt. Express* **2015**, *23*, 18269–18276.
23. Lenski, M.; Heuermann, T.; Wang, Z.; Aleshire, C.; Gaida, C.; Jáuregui, C.; Limpert, J. Highly efficient, in-band pumped, thulium-doped, Q-switched fiber laser. In Proceedings of the Fiber Lasers XXI: Technology and Systems, San Francisco, CA, USA, 29 January–1 February 2024; SPIE: Washington, DC, USA, 2024; Volume 12865, p. 128650T.
24. Zhang, L.; Zhang, J.; Sheng, Q.; Li, Y.; Shi, C.; Shi, W.; Yao, J. 1.7-µm Tm-doped fiber laser intracavity-pumped by an erbium/ytterbium-codoped fiber laser. *Opt. Express* **2021**, *29*, 25280–25289.
25. Braglia, A.; Califano, A.; Liu, Y.; Perrone, G. Architectures and components for high power CW fiber lasers. *Int. J. Mod. Phys. B* **2014**, *28*, 1442001.
26. Braglia, A.; Olivero, M.; Neri, A.; Perrone, G. Fabrication of pump combiners for high-power fiber lasers. In Proceedings of the Fiber Lasers VIII: Technology, Systems, and Applications, SPIE LASE 2011, San Francisco, CA, USA, 24–27 January 2011; International Society for Optics and Photonics (SPIE): Washington, DC, USA, 2011; Volume 7914, p. 79142V.
27. Tao, M.; Huang, Q.; Yu, T.; Yang, P.; Chen, W.; Ye, X. Cross relaxation in Tm-doped fiber lasers. In Proceedings of the 2nd International Symposium on Laser Interaction with Matter (LIMIS 2012), Xi'an, China, 9–12 September 2012; International Society for Optics and Photonics (SPIE): Washington, DC, USA, 2013; Volume 8796, p. 87961W.
28. Stoneman, R.C.; Esterowitz, L. Intracavity-pumped 2.09-μm Ho:YAG laser. *Opt. Lett.* **1992**, *17*, 736–738. [PubMed]
29. Schellhorn, M.; Hirth, A.; Kieleck, C. Ho:YAG laser intracavity pumped by a diode-pumped Tm:YLF laser. *Opt. Lett.* **2003**, *28*, 1933–1935. [PubMed]
30. Duan, X.M.; Guo, X.S.; Yao, B.Q.; Zheng, L.H.; Su, L.B. Efficient Ho:CaF2 laser intracavity-pumped by a Tm:LuAG laser in-band pumped at 1.6 µm. *Laser Phys. Lett.* **2018**, *15*, 095802.
31. Braglia, A.; Califano, A.; Liu, Y.; Olivero, M.; Perrone, G.; Orta, R. Devices and pumping architectures for 2 µm high power fiber lasers. In Proceedings of the Laser Sources and Applications II, Brussels, Belgium, 1 May 2014; International Society for Optics and Photonics (SPIE): Washington, DC, USA, 2014; Volume 9135, p. 91350O.
32. Beccaria, A.; Bellone, A.; Mirigaldi, A.; Serafini, V.; Olivero, M.; Vallan, A.; Perrone, G. Temperature monitoring of tumor hyperthermal treatments with optical fibers: Comparison of distributed and quasi-distributed techniques. *Opt. Fiber Technol.* **2020**, *60*, 102340.
33. Mirigaldi, A.; Serafini, V.; Motta, G.; Perrone, G. High-power multi-emitter modules with fiber Bragg grating stabilization. *Proc. SPIE* **2023**, *12403*, 124030L.
34. Serafini, V.; Cavagnetto, M.; Zaimovic, S.; Tanasi, L.M.; Perrone, G. In-fiber stabilization of high-power blue multiemitter modules. In Proceedings of the High-Power Diode Laser Technology XXII, SPIE LASE 2024, San Francisco, CA, USA, 28–30 January 2024; Zediker, M.S., Zucker, E.P., Campbell, J., Eds.; International Society for Optics and Photonics (SPIE): Washington, DC, USA, 2024; Volume 12867, p. 128670C.
35. The MathWorks, Inc. 2024. MATLAB Version: 24.1 (R2024a). Available online: https://www.mathworks.com (accessed on 31 December 2024).
36. Available online: https://www.rp-photonics.com/rp_fiber_power.html (accessed on 31 December 2024).
37. Tao, M.; Yang, P.L.; Huang, Q.J.; Yu, T.; Ye, X.S. Parameters Determination and Theoretical Modeling of Tm-doped Fiber Lasers. *Key Eng. Mater.* **2013**, *552*, 349–355.

38. Burns, M.D.; Shardlow, P.C.; Barua, P.; Jefferson-Brain, T.L.; Sahu, J.K.; Clarkson, W.A. 47 W continuous-wave 1726 nm thulium fiber laser core-pumped by an erbium fiber laser. *Opt. Lett.* **2019**, *44*, 5230–5233.
39. Panitzek, D.; Romano, C.; Eichhorn, M.; Kieleck, C. Slope efficiency improvement of a core-pumped thulium-doped fibre laser. In Proceedings of the Fiber Lasers and Glass Photonics: Materials through Applications IV, Strasbourg, France, 8–12 April 2024; Taccheo, S., Cicconi, M.R., Jäger, M.L., Eds.; International Society for Optics and Photonics (SPIE): Washington, DC, USA, 2024; Volume 10406, p. 104060B. [CrossRef]
40. Chun, S.I. A Novel Treatment of Acne Vulgaris Using a 1927 nm Fractional Thulium Laser: A Case Series. *Clin. Cosmet. Investig. Dermatol.* **2024**, *17*, 1931–1942. [CrossRef] [PubMed]